SCIENCE CHINA
Technological Sciences

September 2010 Vol.53 No.9: 2388–2396
doi: 10.1007/s11431-010-4057-6

Experimental study on filtering, transporting, concentrating and focusing of microparticles based on optically induced dielectrophoresis

ZHU XiaoLu, YIN ZhiFeng, GAO ZhiQiang & NI ZhongHua*

Jiangsu Key Laboratory for Design and Manufacture of Micro-Nano Biomedical Instruments, Southeast University, Nanjing 211189, China

Received November 19, 2009; accepted March 11, 2010

The key problem to be solved for the dielectrophoresis (DEP) application is to provide dynamically reconfigurable microelectrodes and low-cost methodology for bioparticle manipulation. The emergence of optically induced DEP (ODEP) based on photoconductive effect provides a potential solution for the above problem. In this paper, an ODEP chip is designed and fabricated, and the corresponding experimental platform was established, whereupon four types of particle manipulation regimes–filtering, transporting, concentrating and focusing based on ODEP are experimentally demonstrated and the operating performances are quantitatively analyzed. The experiment results show that the functions and performances of ODEP manipulation are heavily dependent on the geometrical shape, scales and speed of optical patterns, actuating signal frequency and the electric conductivity of the solution. The manipulation efficiency can increase by more than 50% via increasing the optical line width. Moreover, the efficiency is obviously affected by the inclination angle of the optical oblique lines in the manipulation of particle focusing. Additionally, the maximum velocity of particles increases with the increment of the inside radius and the thickness of the optical trapping ring. Particle manipulation efficiency is always related to signal frequency and solution conductivity, and empirically, satisfactory performance and high efficiency are obtained when the solution electric conductivity ranges from 5×10^{-4} S/m to 5×10^{-3} S/m.

optically-induced dielectrophoresis, particle manipulation, filtering, transporting, concentrating, focusing

Citation: Zhu X L, Yin Z F, Gao Z Q, et al. Experimental study on filtering, transporting, concentrating and focusing of microparticles based on optically induced dielectrophoresis. Sci China Tech Sci, 2010, 53: 2388–2396, doi: 10.1007/s11431-010-4057-6

1 Introduction

Most of materials can be polarized to various degrees in an applied electric field. If a nonuniform electric field is imposed on a micro/nano particle, the two poles of the polarized particle will experience unequal and opposite electric forces during its interaction with the nonuniform electric field. Thus, the particle will be subject to a net electric force, which is called dielectrophoresis (DEP) [1]. The manipulation technique based on DEP [2–4] is easy-to-use and requires no moving parts thus can realize massively paralleled active non-contact manipulation for particles [5, 6]. Therefore, the manipulation of micro/nano bio-particles based on DEP is becoming a major enabling technology in filtering [7–9], concentrating [10–12], transporting [13, 14] and flow focusing [6, 15, 16] for microparticles.

However, the above handling approaches based on DEP technology require to design and fabricate complex electrode structures to achieve complex and versatile manipulations of the micro/nano bio-particles. Moreover, the microelectrodes in the previous work lack flexibility and cannot provide real-time alterable electrode-patterns for diverse manipulation requirements. Further, the microelectrodes

*Corresponding author (email: nzh2003@seu.edu.cn)

involve complicated manufacturing process and high cost [2–8, 17–19] . Therefore, on the basis of retaining the advantages of traditional DEP, how to improve the electrodes' flexibility and reconfigurability, and how to cut the manufacturing cost of electrodes have become the key concern in the application of DEP. The proposal of optically induced DEP (ODEP) [20] based on photoconductive effect offered a potential option for the design of highly flexible and real-time reconfigurable optical micro-electrodes [21, 22].

As this research is just emerging in the international arena [21–23], manipulation regimes such as filtering, transporting, parallel concentrating, fluidic focusing, etc. involved in the biomedical testing chip system have not been systematically studied. Meanwhile, there are no relevant reports for systematically analyzing the key factors affecting the ODEP manipulation performance based on experimental results.

The design and manufacturing of an ODEP chip, manipulation patterns and controlling regimes are presented in this paper. Moreover, a detailed study is conducted to the manipulation regimes including filtering, transporting, concentrating and focusing based on ODEP. Furthermore, the relations among the ODEP manipulating performances, optical pattern parameters, signal frequency and liquid conductivities are also experimentally investigated.

2 Experiment setup and method

2.1 ODEP micro device

To fabricate photoconductive layer of ODEP chip (as shown in Figure 1(a)), 50-nm doped hydrogenated amorphous silicon (n+*a*-Si:H), 1.5-μm intrinsic *a*-Si:H and 25-nm silicon carbide (SiC_x) passivation layer were consecutively deposited by plasma enhanced chemical vapor deposition (PECVD) method on the bottom ITO- (indium tin oxide) coated glass at 200°C. The n^+ *a*-Si:H was deposited from a gas ratio of 1% PH_3 in SiH_4, then the intrinsic *a*-Si:H was deposited from a gas mixture containing SiH_4 and H_2. Afterwards, the SiC_x layer was deposited by a SiH_4, CH_3, and N_2 mixture. After that, the ITO layer for bias connections was exposed via reactive ion etch (RIE), as shown in Figure 1(a). The photoconductive layer of the chip consisted of n^+ *a*-Si:H layer, intrinsic *a*-Si:H layer and SiC_x layer (as shown in Figure 1(b)). The n^+ *a*-Si:H layer was used as both a transitionary and adhesive layer from the intrinsic *a*-Si:H layer to the bottom ITO-coated glass. During chip packaging, firstly, a double-faced adhesive tape with a thickness of about 100 μm was pasted on the four edges of the photoconductive surface to form a microchamber with a scale of about 15 mm×8 mm. Then a droplet of about 8–10 μL containing microsphere particles was dripped into the microchamber using a pipettor. Lastly, the top ITO-glass slide was placed onto the roof of the microchamber to make the microchamber sealed as shown in Figure 1(b). In the whole

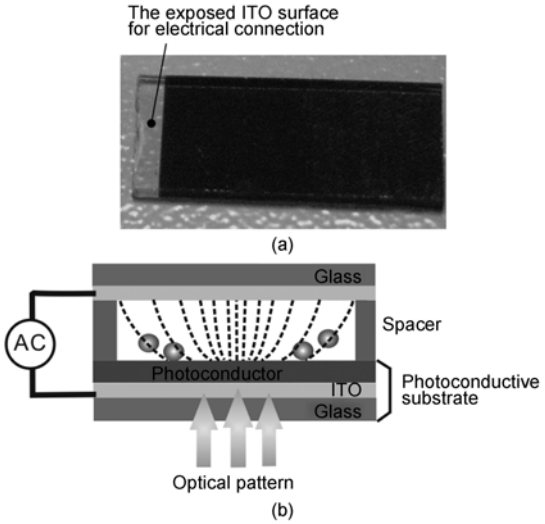

Figure 1 Schematic diagram of the ODEP chip. (a) Photograph of the photoconductive substrate; (b) structure diagram of the ODEP chip.

DEP chip, a 100-μm insulating spacer was used to maintain the gap between the upper ITO film and lower photoconductive layer (see Figure 1(b)). Microparticles were suspended in the solution in the microchamber. The alternating current (AC) voltage (provided by the signal generator) supplied between the top and bottom ITO layers served as the energy source for manipulating particles.

2.2 Principle of the ODEP micro device

For the fabricated ODEP chip as shown in Figure 1(b), the photoconductor has a high electric impedance(about 10^{-6} S/m) prior to illumination, so at this time the most of the applied voltage drops across the photoconductive layer, which causes a weak, uniform electric field inside the liquid layer. At this state, no ODEP force generates. When a projected light source hits the amorphous silicon layer, electron-hole pairs are excited, thus decreasing the impedance of the photoconductive layer by about 5000 times, and the electrical conductivity of the photoconductor is about 5×10^{-3} S/m. At this state, the virtual electrodes are formed in the photoconductor and the voltage drop across the liquid layer in the illuminated area is much higher than that in the dark area. Consequently, the bright-dark pattern induces a nonuniform electric field in this device. The dense electric filed lines appear at the illuminated areas and the sparse field lines appear at the dark areas as shown in Figure 1(b). Then a DEP force exerting on microparticles will be induced in the liquid chamber and the time-averaged DEP force acting on the spherical particle suspended in liquid chamber can be described as follows [1],

$$\left\langle \boldsymbol{F}_{\mathrm{DEP}} \right\rangle = \pi R^3 \varepsilon_{\mathrm{m}} \,\mathrm{Re}\left[\frac{\tilde{\varepsilon}_{\mathrm{p}} - \tilde{\varepsilon}_{\mathrm{m}}}{\tilde{\varepsilon}_{\mathrm{p}} + 2\tilde{\varepsilon}_{\mathrm{m}}} \right] \nabla E^2, \tag{1}$$

where R is the particle radius, E is the amplitude of electric

field, $\tilde{\varepsilon}_p$ and $\tilde{\varepsilon}_m$ are the complex permittivities of the particle and suspending medium, respectively, $\tilde{\varepsilon}_p = \varepsilon_p - j\sigma_p/\omega$, and $\tilde{\varepsilon}_m = \varepsilon_m - j\sigma_m/\omega$. Here σ_p and σ_m are ohmic electrical conductivities of the particle and liquid medium, respectively; ε_p and ε_m are the permittivities of the particle and liquid medium; ω is angular frequency of the electric field. In eq. (1), the expression in brackets $(\tilde{\varepsilon}_p - \tilde{\varepsilon}_m)/(\tilde{\varepsilon}_p + 2\tilde{\varepsilon}_m)$ is referred to as the Clausius-Mossotti (CM) factor. When Re[f_{CM}]>0, positive DEP occurs and particles move toward high field regions; when Re[f_{CM}]<0, negative DEP occurs and parti- cles move toward weak field regions. The particles in the liquid layer also undergo the opposing Stokes' drag [1], as

$$\boldsymbol{F}_{drag} = -6\pi\eta RV, \tag{2}$$

where V is the particle velocity, and η is the dynamic viscosity of the liquid.

2.3 Experimental platform and operation

For our experimental setup as shown in Figures 2(a) and (b), a charge-coupled device camera (the Imaging Source Europe GmbH, Germany) attached to the upright microscope (Nikon ECLIPSE 50i) observation port acquired the particle image through an objective lens from the top of the optoelectronic micro device. The DMD projecting system contained digital micro mirrors with a scale of 10.8 μm ×10.8 μm and corresponding electrical driver board, which was modified from a commercial projector with a resolution of 1024×768 pixels. This DMD-based projector was controlled by computer. The dynamic optical patterns generated by the projector was collimated, collected by a set of lens and reflected through the reflector at 45° to the horizontal and then directed into a 10× optical pattern condenser. Finally, the optical micro patterns were projected onto the photoconductor. By using the optical micropattern control and monitoring software developed by our group (software copyright registration No. 2009SR02775), the real-time reconfiguration and dynamic control of the optical patterns were available for the application of filtering, transporting, concentrating, and focusing of microparticles. The optical micro patterns can be arbitrarily varied in real time, which exactly embodies the flexibility of the optical virtual electrodes.

Additionally, these four types of manipulations in the ODEP microfluidic chip were all accompanied by a phenomenon which resulted in the manipulation failure. We call this phenomenon desynchronization (DS). When the velocity of the optical pattern gradually increases, the velocity of the particle undergoing ODEP force and Stokes' drag force increases correspondingly until the ODEP force is no longer large enough to maintain the synchronization between the particle and the optical pattern, and the particle will lag behind the optical pattern. Before the particle desynchronizes, there is a maximum synchronous velocity (MS-velocity) [24]. The DS process is presented, as shown in Figure 3. As shown in Figure 3(a), ring center was the initial position of the particle and then the particle was lagged to the inward flange of the ring (see Figure 3(b)) when the ring's velocity increased to the threshold value (MS-velocity). Lastly, while the ring moved faster and faster, the particle was not able to follow the ring's movement and was left behind the ring (Figures 3(c) and (d)). A particle reaches its MS-velocity when the maximum value of the horizontal driving DEP force is available in the optical trap pattern, and at this state, the relative position between the moving particle and moving light pattern is close

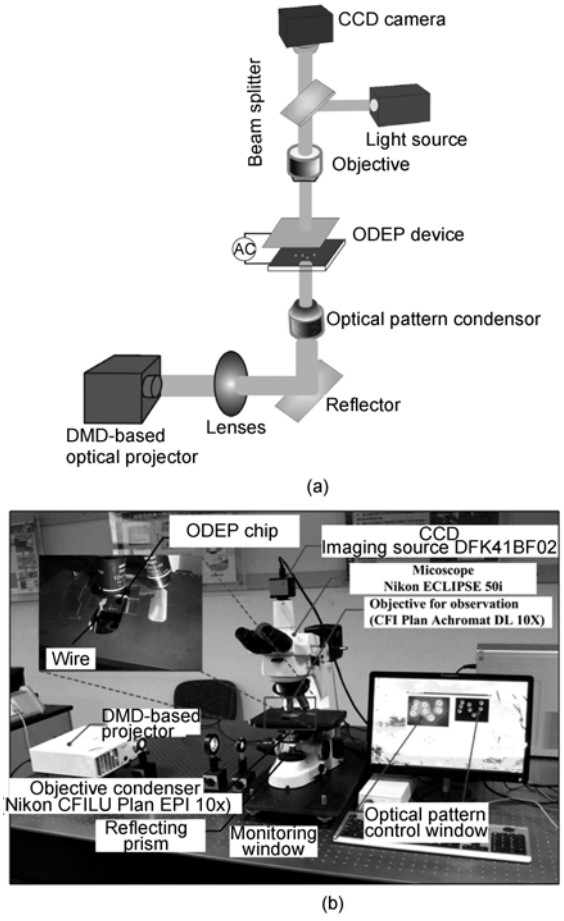

Figure 2 Experiment setup for the real-time controllable ODEP platform. (a) Schematic diagram of the ODEP platform; (b) photograph of the virtual electrode control platform for ODEP experiment.

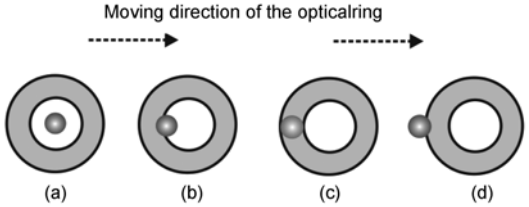

Figure 3 The desynchronization process of ODEP.

enough (as shown in Figure 3(b)).

Because of the characteristics of electrical neutrality of the microscale bioparticles, the test particles used in this experiment were the 30-μm-diameter and 50-μm-diameter polystyrene microsphere particles (Duke Scientific Corp.) and 17–21 μm in diameter pollen grains (Duke Scientific Corp). These particles were suspended in deionized water, which had an electrical conductivity of about 1.5×10^{-3} S/m.

2.4 Electric filed simulation for the ODEP chip

Based on the above ODEP chip and the experiment setup, the electric field distribution in the ODEP chip is strongly perturbed after the photoconductor in ODEP chip is selectively illuminated by the optical patterns. Here, the electric potential is denoted by symbol ϕ. The field distribution at the bright-dark areas in the microchamber of the ODEP chip can be achieved by solving the Laplace equation $\nabla^2\varphi = 0$ via a finite element program package (Comsol Multiphysics 3.2a). The simulation results for the squared-field strength distribution in the cross section of the chip are shown in Figure 4. The illuminated area length along the horizontal direction is set as 40 μm in both Figures 4(a) and (b). The isolines in Figure 4 indicate the squared field strength (E^2). The largest E^2 exists near the bottom of the microchamber while the smallest E^2 exists at the area far from the illuminated area. According to eq. (1), when the particle undergoes negative DEP (Re[f_{CM}]<0), the DEP force is in the opposite direction of the gradient of the E^2, i.e., the particle will be repelled from the strong field areas. Specifically, the particles will be repelled from the junction of the bright and dark area with the strongest field near the bottom surface of the microchamber. Therefore, when the junction of the bright and dark area is moving from the left position (shown in Figure 4(a)) to the right position (shown in Figure 4(b)), the particle at the right side of the bright area will also be repelled towards the right. That is the basic principle of the optical pattern driving particles in ODEP chip.

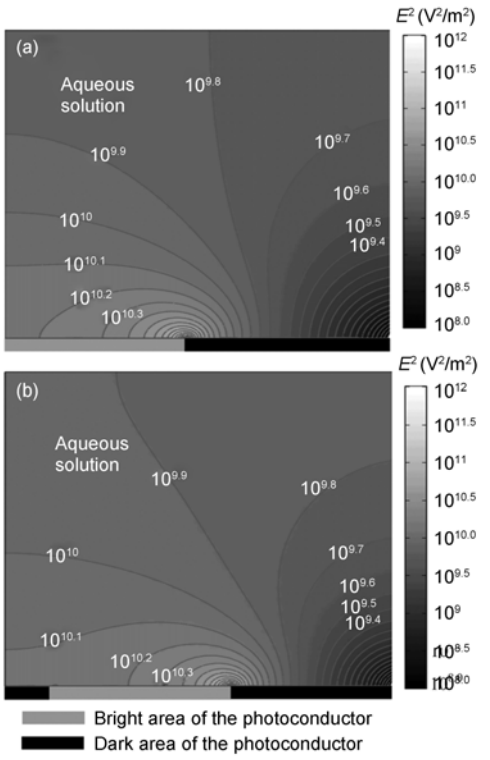

Figure 4 The distribution of the squared electric field in the cross section of the microchamber in the ODEP chip.

3 Results and discussion

3.1 Filtering

Usually, the non-target stuff or microparticles in the raw sample should be filtered firstly in the pretreatment for the sample. The filtering experiment was implemented via the scanning of an optical line as shown in Figure 5. In the filtering experiment, with an applied $20V_{pp}$ at 600 kHz, the normal pollen grains with diameters of 17–21 μm and most of the 30-μm diameter polystyrene particles were driven by the optical line with a thickness of about 70 μm towards the bottom area of the view as shown in Figure 5. In contrast, the degenerative pollen grains and few polystyrene particles were left in their original positions (look at the range confined by the dotted lines), which could realize the filtering function. This separation phenomenon in the filtering experiment is probably because the particles left behind are difficult to be polarized relative to the normal ones, which resulting in much smaller DEP force for the abnormal. As to the few polystyrene particles left behind the optical line, another reasonable explanation maybe that these particles were pushed away by the interacting force among the individual particles when the scanning optical line drived the particles. The velocity of the optical lines in Figure 5 was about 14 μm/s.

As long as the optical line velocity did not exceed the MS-velocity of the normal particles (i.e. maximum filtering velocity), the filtering function could be achieved. If the optical line velocity exceeded the MS-velocity, all particles would be left behind the scanning optical line, which made the filtering unavailable. The relations between the optical line width and the maximum filtering velocity at different AC signals are shown in Figure 6. The filtering efficiency increased by 50%–60% when the optical line width grew from 30 μm to 90 μm. This filtering experiment demonstrated the feasibility of the ODEP filtering. Moreover, a longer and thicker optical line led to a broader filtering area and a higher filtering efficiency. The ODEP filtering can meet many specific filtering requirements by just changing the shape, scale and velocity of the optical pattern, which is much more flexible than the conventional filtering. As presented in Figure 6, a larger applied voltage leads to a larger maximum filtering velocity because DEP force increases

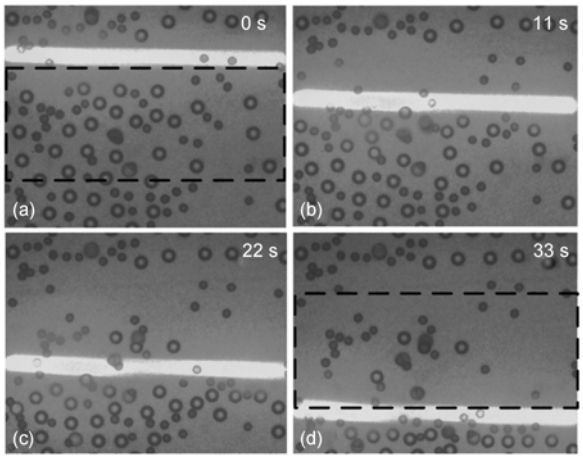

Figure 5 Snapshots of the filtering process in the way that a scanning light line moved from the top of the viewing field to the bottom of the view (Degenerative pollen grains and few polystyrene particles were left behind the light line while the normal particles were able to be driven by the scanning light line).

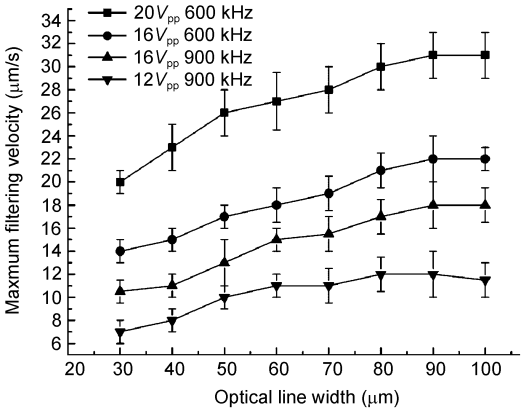

Figure 6 The relation between the optical line width and the maximum filtering velocity.

with the raise of applied voltage. However, the maximum filtering velocity decreased when the frequency varied from 600 kHz to 900 kHz. That is because the impedance of the aqueous layer of ODEP chip decreased with the increase of frequency due to the electrical capacitive effect implied in aqueous layer, and thus the voltage across the aqueous layer correspondingly decreased, resulting in a smaller DEP force.

3.2 Transporting

ODEP can trap individual particles and then transport the particles to anticipant positions and the motion paths can be programmed and controlled. As shown in Figure 7, under the AC condition of $20V_{pp}$ and 1 MHz, two particles with 30-μm diameters were trapped individually and programmed motion paths were imposed on the two particles (particle 1 and particle 2 shown in Figure 7). These two particles were able to move simultaneously depending on their respective routings. Figure 7 presents the ability of transporting particles parallelly via ODEP. The optical patterns can be controlled by the ODEP controlling software developed by ourselves. The two optical rings in Figure 7 have an external diameter of about 150 μm and an interior diameter of about 40 μm. The polystyrene particles were always trapped by the illuminated optical rings during the transporting. Particle 1 and particle 2 were always following the motion of the optical rings from the initial positions at the upper area of the snapshot to the terminative area of the snapshot. During the transporting, the two particles moved simultaneously and always dodged each other as shown in Figures 7(b)–(g) until they exchanged their positions and arrived at their own new destinations. Comparing Figures 7(a) and (h), particle 1 and particle 2 switched their positions.

The transporting velocity is a vital evaluating indicator for the transporting performance and efficiency. To achieve

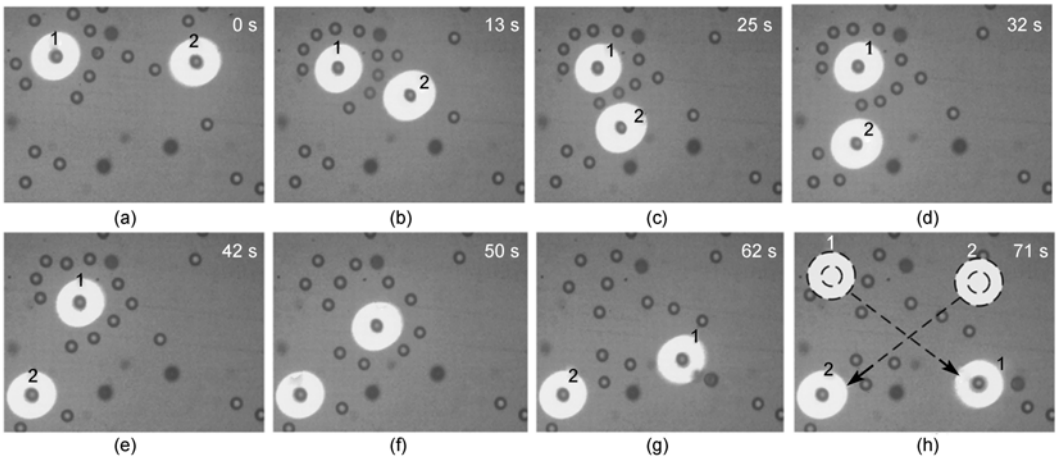

Figure 7 Snapshots of the transporting of two individual polystyrene particles parallelly (Particle 1 and particle 2 were driven towards the underneath of the view field and the left particle and right particle were switched their positions during the downward transporting. The optical rings drawn by dashed lines in (h) indicate the original positions of the two particles).

a distinguished and remarkable feature of the transporting velocity's dependency on the thickness and the inside radius of the trapping ring, we employed the particles with a relatively large diameter (50 μm). Figure 8 shows the MS-velocity of 50-μm-diameter polystyrene particles with respect to the thickness and the internal radius of the optical pattern. When the inside radius of the optical ring was defined as 50 μm, the MS-velocity increased with the ring thickness in a roughly linear fashion. Figure 8(b) reflects the relation between the MS-velocity and the inside radius of the optical trapping ring at a constant thickness of the optical ring. The profile of MS-velocity increases steeply when the inside radius of the light ring is less than 60 μm, but the profile is approximately flat while the inside radius of the optical ring is more than 60 μm. From Figure 8, it is found that at different frequencies, the MS-velocity profiles versus the radius and thickness of light ring have similar tendencies and shapes.

3.3 Concentrating

In many applications, a single particle's reaction with other reagent is very weak but a concentrated population of particles can react with other reagent intensively with obvious phenomena. Therefore, when the raw sample is filtered and transported to the destinations in a specified manner, the isolated particles need concentration for the following detecting step. The experiment presented in Figure 9 demonstrated the concentrating regime of ODEP. The test particles in the experiment were the 30-μm-diameter polystyrene particles. With an applied voltage of $20V_{pp}$ at 900 kHz, at an arbitrary area, the micro light pattern of two collecting bowls (A and B in Figure 9) can be used to collect a population of particles with an arbitrarily set number (see Figures 9(a)–(c)) and can move the trapped particle population to an arbitrary location. For example, the concentrated particles shown in Figure 9(d) could be moved as a whole to the position shown in Figure 9(f). For the movement of A and B as well as the movement of the particle population, a MS-velocity of the optical pattern existed for the concentrating operation.

The time needed for concentrating at the MS-velocity of optical pattern is referred to as the minimum concentrating time (MC-time). Figure 10 shows the relation between the optical linewidth and the minimum concentrating time. Generally, a thicker optical line leads to a higher concentration efficiency and less MC-time. As shown in Figure 10, the MC-time under $16V_{pp}$ voltage is more than that under

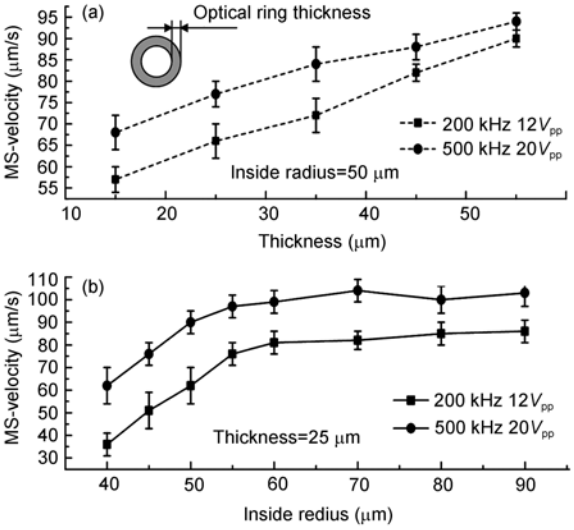

Figure 8 MS-velocities versus the thickness and the inside radius of the optical trapping ring.

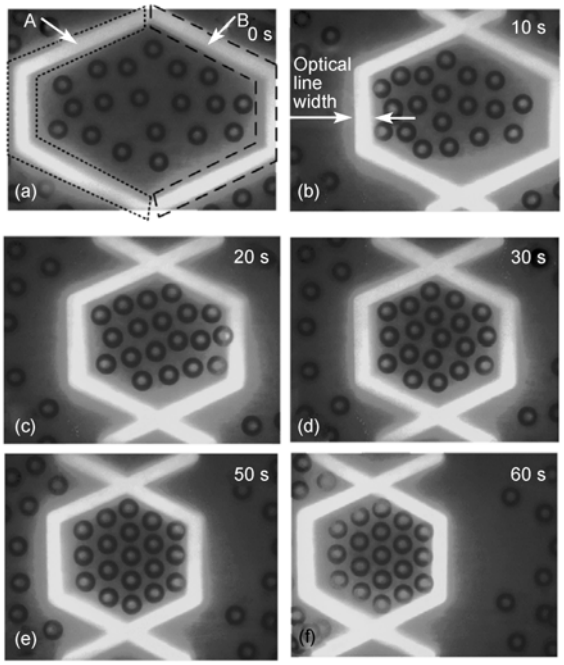

Figure 9 Concentrating procedure for microparticles when the two collecting bowls (A and B) move closer and closer as shown in (a), (b) and (c) (The concentrated particles can entirely move as a whole from the position in (d) to the position in (f)).

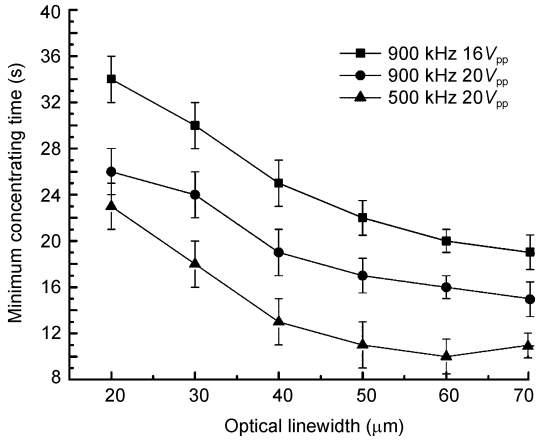

Figure 10 Relations between the width of the optical line and the minimum concentrating time (MC-time) at different AC conditions.

$20V_{pp}$ at the same frequency. The reason is that a lower voltage resulting in lower electric filed strength weakens the magnitude of DEP force, and thus decreases the particle velocity. On the other hand, the MC-time required at 500 kHz is less than that at 900 kHz. This is because the capacitive impedance of the aqueous layer significantly decreases when the signal frequency increases especially when the frequency is higher than 500 kHz, thus leading to lower voltage drop across the aqueous layer. Then the DEP force decreases, leading to slower particle motion and thus a longer MC-time.

3.4 Focusing

Besides concentrating particles, focusing is another post treatment mode. Focusing is mainly used to continuously and automatically count and detect individual particles. The ability to focus particles based on ODEP is demonstrated in Figure 11. In this study, a series of longitudinally symmetric optical oblique line-array were projected at oblique angles on the photoconductive layer to focus the microparticles in a straight sample flow. The optical linewidth and the gap between adjacent optical lines were set as 40 μm and 50 μm, respectively. The inclination angle for each virtual electrode was about 30° (refer to Figure 11(a)). The optical oblique line-array was moving relatively to the particles in 30-μm diameter when the microscope stage carrying the ODEP device moved horizontally along the direction of the virtual channel. This relative motion could be regarded as the flow of particles relative to optical patterns. With an applied $24V_{pp}$ at 600 kHz, the microparticles underwent negative ODEP force which drove particles away from the virtual electrodes (optical oblique lines), and thus the horizontally moving particles swam along the oblique light lines and then swam into the virtual channel. In the virtual channel particles were focused into a straight particle line (see Figures 11(e) and (f)). Note that there was not any substantial channel flow to assist the focusing of the microparticles.

The relative velocity between the particles and optical patterns for particle focusing had a maximum value (V_{fmax}) which reflects the focusing efficiency. If the relative velocity is larger than V_{fmax}, the particle in the ambient area around the virtual channel will horizontally move over the optical lines, resulting in the failure of particle focusing. As shown in Figure 12, the optical linewidth d and its inclination angle α are the two main factors influencing the value of $V_{fmax.}$ The focusing efficiency grows by about 50% when the optical linewidth increases from 30 μm to 70 μm (Figure 12(a)). When the inclination angle α increases from 20° to 70°, the focusing efficiency grows by about 3 times (Figure 12(b)). This is because the component force along the oblique optical line increases with the increase of α, leading to larger velocity of particles. Moreover, at the same magnitude of voltage, the particle velocity at 600 kHz is larger than that at 1 MHz as shown in Figure 12. The

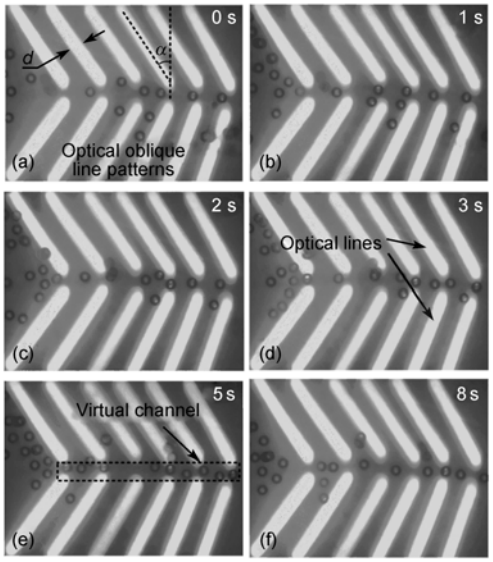

Figure 11 Microparticles are focused into a narrow particle line by "virtual electrodes" projected onto the photoconductive layer to generate a negative ODEP force (Original state (a) is the random spatial distribution of microparticles. While the microscope stage that carries the ODEP device was moving, the random-located particles were gradually forming a straight particle line (shown in (b), (c), (d)) and after about 5 s, the particle line was becoming stable as shown in (e) and (f)).

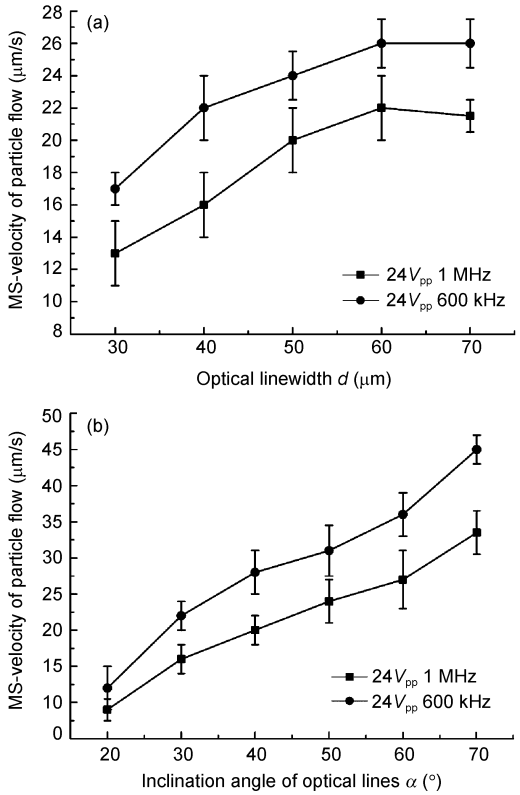

Figure 12 (a) Relations between the MS-velocity of the particle flow and the optical linewidth(inclination angle α=30° and the optical line gap was about 50 μm); (b) relations between the MS-velocity of the particle flow and the inclination angle of optical lines (d=40 μm, optical line gap was about 50 μm).

reason for that is the capacitive impedance of the aqueous layer decreases from 600 kHz to 1 MHz, and thus the voltage drop across the aqueous layer decreases, resulting in the decrease of DEP force and particle MS-velocity.

3.5 Influence of signal frequency and solution conductivity on the CM factor

These particle manipulation regimes can be integrated in a single chip system. These ODEP manipulation functions benefit much from the flexible design of the light patterns. Meanwhile, the manipulation efficiency is not only related to optical patterns, but also much related to the frequency, voltage and the conductivity of the medium. The essential reason for the frequency-dependent response of particles is that the CM factor varies with the frequency. For the polystyrene beads, surface conductivity should be taken into account because the beads have a surface conductivity of about 2×10^{-9} S/m that is significantly larger than the bulk conductivity of only 1×10^{-16} S/m. The suspending liquid for particles has a permittivity of about $78.5\varepsilon_0=6.95\times10^{-10}$ F/m. Figure 13 shows the curves of Re[f_{CM}] with respect to frequency for the particles with 50-μm and 30-μm diameters. As shown in Figure 13, with the increase of frequency, the Re[f_{CM}] value decreases until it is down to constant. For a certain frequency, Re[f_{CM}] decreases with the raise of the solution conductivity. However, when the solution conductivity exceeds 5×10^{-4} S/m, the Re[f_{CM}] varies slowly in a nonlinear manner.

When the frequency is below 100 kHz, Re[f_{CM}] decreases significantly with the raise of solution conductivity at a certain frequency (the minimum value is –0.5). When the frequency is higher than 300 kHz, the solution conductivity does not influence Re[f_{CM}] remarkably (refer to Figure 13). Excessively low solution conductivity will give rise to positive DEP (Re[f_{CM}]>0) or very small magnitude values of Re[f_{CM}], which does not benefit the negative ODEP manipulation in these experiments. A larger solution conductivity will lead to a larger magnitude of Re[f_{CM}] when Re[f_{CM}]<0. Nevertheless, an excessive high solution conductivity will result in the decrease of aqueous layer impedance, and then decrease the voltage drop across the aqueous layer, which causes a much smaller DEP force. After several experimental tests, it was found that the solution conductivity between 5×10^{-4} S/m and 5×10^{-3} S/m was a compromise choice.

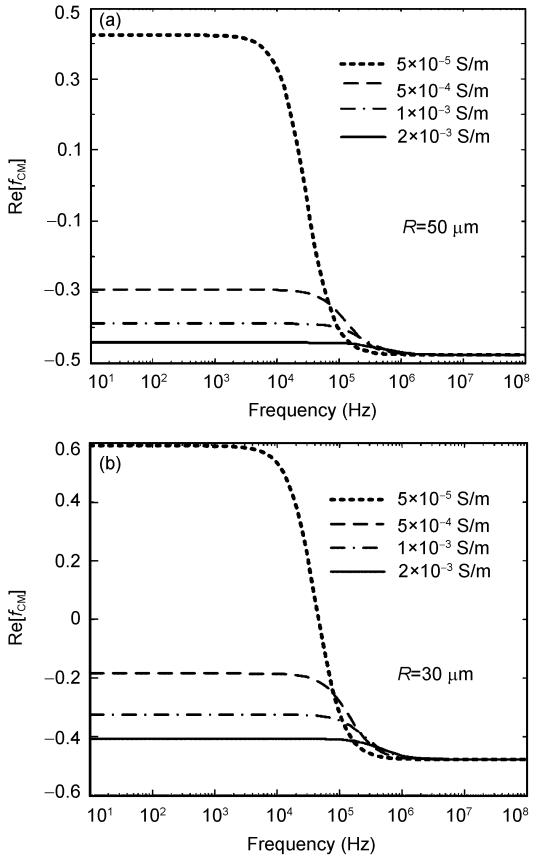

Figure 13 Value of Re[f_{CM}] as a function of the signal frequency. (a) Re[f_{CM}] curves for polystyrene particles with a diameter of 50 μm; (b) Re[f_{CM}] curves for polystyrene particles with a diameter of 30 μm.

4 Conclusions

In this paper, the optical micro patterns for filtering, parallelly transporting, concentrating and focusing of microparticles were designed, and the scanning filtering, multiparticle parallel transportation, particle concentration at an appointed microarea and the focusing for signal particle queue were demonstrated experimentally.

The filtering experiment indicated that the MS-velocity of particles increased with the increase of the optical linewidth. The filtering efficiency increased by 50%–60% when the optical line width grew from 30 μm to 90 μm. For the transporting experiment, the particle MS-velocity increased with the growing of thickness and inside radius of the trapping optical ring. The particle MS-velocity increased steeply when the inside radius of optical ring was less than 60 μm, but approximately flat when the inside radius of optical ring was more than 60 μm. For the concentrating experiment, the MC-time decreased with the increase of the optical linewidth, and the concentrating efficiency grew by 50%–70% when the width of the optical linewidth increased from 20 μm to 70 μm. Additionally, the concentrating efficiency at 500 kHz was higher than that at 900 kHz. For the focusing experiment, the MS-velocity V_{fmax} increased with the increase of optical line width d and its inclination angle α. The focusing efficiency grew by about 50% when the optical linewidth increased from 30 μm to 70 μm. When the inclination angle α increased from 20° to 70°, the focusing efficiency grew by about three times.

For polystyrene particles, the manipulation efficiency

had nonlinear relations with the signal frequency and solution conductivity, and both satisfactory performance and high efficiency were obtained when the solution conductivity was between 5×10^{-4} S/m and 5×10^{-3} S/m.

This work was supported by the National High Technology Research and Development Program of China ("863" Program) (Grant No. 2009AA04Z310) and the National Natural Science Foundation of China (Grant Nos. 30770553, 50805022).

1 Morgan H, Green N G. AC Electrokinetics: Colloids and Nano-particles (Microtechnologies and Microsystems). Philadelphia: Research Studies Press, 2003
2 Medoro G, Guerrieri R, Manaresi N, et al. Lab on a chip for live-cell manipulation. IEEE Des Test Comput, 2007, 24(1): 26–36
3 Wang X B, Huang Y, Gascoyne P R C, et al. Dielectrophoretic manipulation of particles. IEEE Trans Ind Appl, 1997, 33(3): 660–669
4 Doh I, Cho Y H. A continuous cell separation chip using hydrodynamic dielectrophoresis (DEP) process. Sens Actuator A-Phys, 2005, 121(1): 59–65
5 Gascoyne P R C, Vykoukal J V. Dielectrophoresis-based sample handling in general-purpose programmable diagnostic instruments. Proc IEEE, 2004, 92(1): 22–42
6 Cheng I F, Chang H C, Hou D, et al. An integrated dielectrophoretic chip for continuous bioparticle filtering, focusing, sorting, trapping, and detecting. Biomicrofluidics, 2007, 1: 021503
7 Hawkins B G, Smith A E, Syed Y A, et al. Continuous-flow particle separation by 3D insulative dielectrophoresis using coherently shaped, DC-biased, AC electric fields. Anal Chem, 2007, 79(19): 7291–7300
8 Flanagan L A, Lu J, Wang L, et al. Unique dielectric properties distinguish stem cells and their differentiated progeny. Stem Cells, 2008, 26(3): 656–665
9 Pethig R. Dielectrophoresis: using inhomogeneous ac electrical fields to separate and manipulate cells. Crit Rev Biotechnol, 1996, 16(4): 331–348
10 Schonfeld F, Griebel A, Konrad R, et al. Development of a μ-concentrator using dielectrophoretic forces. J Assoc Lab Autom, 2002, 7(6): 130–134
11 Gagnon Z, Chang H C. Aligning fast alternating current electroosmotic flow fields and characteristic frequencies with dielectrophoretic traps to achieve rapid bacteria detection. Electrophoresis, 2005, 26(19): 3725–3737
12 Wu J, Ben Y X, Battigelli D, et al. Long-range AC electroosmotic trapping and detection of bioparticles. Ind Eng Chem Res, 2005, 44(8): 2815–2822
13 Desai A, Lee S W, Tai Y C. A MEMS electrostatic particle transportation system. Sens Actuator A-Phys, 1999, 73(1-2): 37–44
14 Crews N, Darabi J, Voglewede P, et al. An analysis of interdigitated electrode geometry for dielectrophoretic particle transport in micro-fluidics. Sens Actuator B-Chem, 2007, 125(2): 672–679
15 Fu L M, Yang R J, Lin C H, et al. Electrokinetically driven micro flow cytometers with integrated fiber optics for on-line cell/particle detection. Anal Chim Acta, 2004, 507(1): 163–169
16 Yao B, Luo G A, Feng X, et al. A microfluidic device based on gravity and electric force driving for flow cytometry and fluorescence activated cell sorting. Lab Chip, 2004, 4(6): 603–607
17 Durr M, Kentsch J, Muller T, et al. Microdevices for manipulation and accumulation of micro- and nano-particles by dielectrophoresis. Electrophoresis, 2003, 24(4): 722–731
18 Park S, Beskok A. Alternating current electrokinetic motion of colloidal particles on interdigitated microelectrodes. Anal Chem, 2008, 80(8): 2832–2841
19 Fatoyinbo H O, Hoeftges K F, Hughes M P. Rapid-on-chip determination of dielectric properties of biological cells using imaging techniques in a dielectrophoresis dot microsystem. Electrophoresis, 2008, 29(1): 3–10
20 Chiou P Y, Ohta A T, Wu M C. Massively parallel manipulation of single cells and microparticles using optical images. Nature, 2005, 436(7049): 370–372
21 Hwang H, Lee D H, Choi W J, et al. Enhanced discrimination of normal oocytes using optically induced pulling-up dielectrophoretic force. Biomicrofluidics, 2009, 3: 014103
22 Ni Z, Yi H, Zhu S, et al. Research on critical technology of micro/nano bioparticles manipulation platform based on light-induced dielectrophoresis. Sci China Ser E-Tech Sci, 2009, 52(10): 2831–2839
23 Zhu X, Yi H, Ni Z, et al. Automatic separation of microscopic particles via optoelectronic chip and associated platform. In: Int Conf Mechatron & Automat. Changchun: IEEE, 2009
24 Zhu X, Yi H, Ni Z. Frequency-dependent behaviors of individual microscopic particles in an optically induced dielectrophoresis device. Biomicrofluidics, 2010, 4: 013202